Hindawi
Shock and Vibration
Volume 2021, Article ID 3726306, 9 pages
https://doi.org/10.1155/2021/3726306

Research Article

Pressure Load Characteristics of Explosions in an Adjacent Chamber

Chuan-hao Wang, Shu-shan Wang, Jing-xiao Zhang, and Feng Ma

State Key Laboratory of Explosion Science and Technology, Beijing Institute of Technology, Beijing 100081, China

Correspondence should be addressed to Feng Ma; kang@bit.edu.cn

Received 17 December 2019; Revised 9 June 2020; Accepted 7 January 2021; Published 22 January 2021

Academic Editor: Yuri S. Karinski

To learn more about dynamite explosions in confined spaces, we focused on the chamber adjacent to the main chamber, the main chamber being the location of the explosion. We investigated the characteristics of two damaging pressure loads: first reflected shock wave and quasistatic pressure. In this work, we analyzed the characteristics of the first reflected shock wave and the quasistatic pressure formed by the explosion of the chamber charge. Simulated chamber explosion experiments were carried out, where high-frequency piezoelectric sensors were used to measure the first reflected shock wave, and low-frequency piezo-resistive sensors were used to measure the quasistatic pressure. Valid and reasonable experimental data were obtained, and the experimental values of the pressure load were compared with those calculated from the classical model. The results showed that when the main chamber was partially damaged by the explosion load, the adjacent chambers were not subjected to the shock wave load, and the quasistatic pressure load was less than that in the main chamber. The presence of adjacent chambers did not affect the shock wave load in the main chamber. Using the mass of the explosive and the blast distance as input parameters, the internal explosion shock wave load parameters, including those in adjacent chambers, can be calculated. The presence of the adjacent chamber did not affect the theoretically calculated quasistatic overpressure peak in the main chamber. Using the mass of the explosive and the spatial volume of the chamber as input parameters, the quasistatic pressure load parameters of the internal explosion can be calculated, including those in the adjacent chambers.

1. Introduction

The explosion of dynamite inside a confined space leads to two typical pressure loads: shock wave and quasistatic pressure. Due to the constraint of boundary conditions, the time history of an internal explosion pressure load is much more complicated than that of an external explosion, and it will cause more severe damage [1, 2]. The shock wave is continuously reflected inside the confined space and superimposes at the corners, causing plastic deformation and local fracture of the structure. The first reflected shock wave is decisive, whereas quasistatic pressure is believed to be the deciding factor for structural disintegration and overall destruction based on structural damage and local failure. Therefore, the first reflected shock wave and quasistatic pressure comprise an important basis for analyzing and evaluating the damage effect.

The study of the explosion pressure load in a chamber began during World War II [3]. The initial researchers believed that the reflected shock wave was the main damage load. In the 1960s, quasistatic pressure loads began to receive attention. Books [4–6], reports [7–10], and manuals [11–13] on this topic included the relationship between the two pressure loads mentioned above and the mass and position of the explosive, the volume of the confined space, and the area of pressure relief. The literature also included computation models for the two load parameters in a specific range of applications and the interaction between the pressure load and the structure. These research results have made possible the prediction and evaluation of internal explosion pressure load. In terms of mechanisms, studies on reflected shock waves mainly included theoretical calculations of multiple reflection shock waves [14–16], local

interaction between shock wave and confined space [17–20], research on quasistatic pressure, mainly the calculation of quasistatic pressure load parameters [21–23], effects of postexplosive combustion on quasistatic pressure [24–27], effects of shape and structure of pressure relief hole on quasistatic pressure [28–32], and internal explosion load characteristics of nonideal explosives [33–35]. In contrast to research on single chambers, today's research on the internal explosion pressure load of multichamber structures is inadequate. Multichamber structures are closer to the reality, and the characteristics of internal explosion pressure loads are more complicated. With increasingly greater demand on the destruction capability of internal explosion load and increasing requirements for a structure's anti-internal explosion performance, it has become increasingly important to investigate internal explosion pressure load characteristics of adjacent chambers. In this study, we conducted internal explosion experiments with charges in simulated chambers. Two types of pressure sensors were used to test the reflected shock wave and the quasistatic pressure in synchronized tests. Combined with theoretical analysis and calculation, we studied the characteristics and behavior of pressure loads in an adjacent chamber generated by an explosion in the main chamber.

2. Pressure Load Characteristics of Explosion inside Cabin

When an explosion occurs in a limited space, the explosive will form a high-temperature and high-pressure detonation product as well as rapidly expand the compressed air to form an explosion shock wave in the air. After the explosion shock wave is separated from the explosive product-air interface, the product continues to expand and gradually mixes with the air compressed by the shock wave. Subsequently, the shock wave reaches the boundary of the finite space and is reflected, and the spatial Euler point exhibits a fluctuating process where the peak pressure is continuously attenuated [23]. The average value of such fluctuating pressure is called the quasistatic pressure. For an observation point on a solid wall, the quasistatic pressure starts from the moment the shock wave first arrives and reflects and continues until it reaches its peak when the detonation product is mixed with the original air. Due to the short time frame, the pressure drop caused by the existence of the pressure relief hole and the heat exchange between the gas and the solid walls can be ignored. The quasistatic pressure continues to decrease over time, and this decay process lasts for seconds.

The explosive explodes in the cabin, and the fluctuating pressure reflected on the bulkhead can be decomposed into two kinds of damage pressure loads: the first incident shock wave and the quasistatic pressure. The pressure loads can be analyzed and processed relatively independently. The load parameters of the first incident shock wave include the first peak overpressure, positive pressure action time, and specific impulse. The load parameters of the quasistatic pressure include the peak overpressure of the quasistatic pressure, pressure relief time, and specific impulse. The amplitude of the first incident shock wave is typically on an order of magnitude of 10 MPa and the positive pressure action time is on an order of magnitude of milliseconds, which are typical high-frequency pressure signals. Hence, to test the first incident shock wave, the sensor should have a response frequency of hundreds of kilohertz, and the collector should have a sampling frequency in megahertz. The quasistatic pressure is usually on an order of magnitude of kilopascals, and the pressure relief time is on an order of magnitude of seconds. Moreover, since the quasistatic pressure is the average of the fluctuating pressure, the response frequency of the quasistatic pressure test sensor should be low (kilohertz) to ensure that the data are stable and that it is possible to obtain a smooth test curve [36].

3. Explosion Experiment in Simulated Chambers

3.1. Chamber Structure and Test Method. In order to study the pressure load characteristics of explosion in an adjacent chamber, we conducted explosion tests in simulated chambers. For comparative analysis, two simulated chambers were designed. Simulated chamber 1 was a single-level chamber, and the standard chamber was used to analyze the internal explosion pressure load without an adjacent chamber. Simulated chamber 2 was double-layered, with the upper chamber serving as the main chamber and the lower chamber serving as the adjacent chamber. Simulated chamber 2 was used for analyzing the internal explosion pressure load in the main and adjacent chambers. The total volume of simulated chamber 2 was twice that of simulated chamber 1, and the upper and lower chambers were of the same volume and connected through a prefabricated hole. Figure 1 shows a schematic diagram of the simulated chambers used in the experiment.

Figure 1 shows that, for simulated chamber 1, a total of four test points were located on the two bulkheads at the front and back of the simulated chamber. Test point 1 and test point 2 were located at the geometric center of the front and rear bulkheads, respectively, for acquiring shock wave load data. Test point 3 and test point 4 were located on both sides of test point 2 at the front bulkhead to obtain quasistatic pressure load data. For simulated chamber 2, the upper chamber was the main chamber, and the lower chamber was the adjacent chamber. The test point distribution in the main chamber was the same as that in simulated chamber 1. Test points 5, 6, and 7 were located in the front bulkhead of the lower chamber at locations corresponding to the test points in the upper main chamber. Test point 7 was used to obtain shock wave load data in the lower adjacent chamber, and test points 5 and 6 were used to acquire the quasistatic pressure load in the lower adjacent chamber. The physical layout of the simulated chamber is shown in Figure 2.

As shown in Figure 2(a), the internal dimensions of simulated chamber 1 were $2.4\,\text{m} \times 1.2\,\text{m} \times 0.5\,\text{m}$, the bulkhead thickness was 16 mm, the round hole at the top of the chamber was 120 mm in diameter, and the explosive charge was suspended in an iron frame at the geometric center of

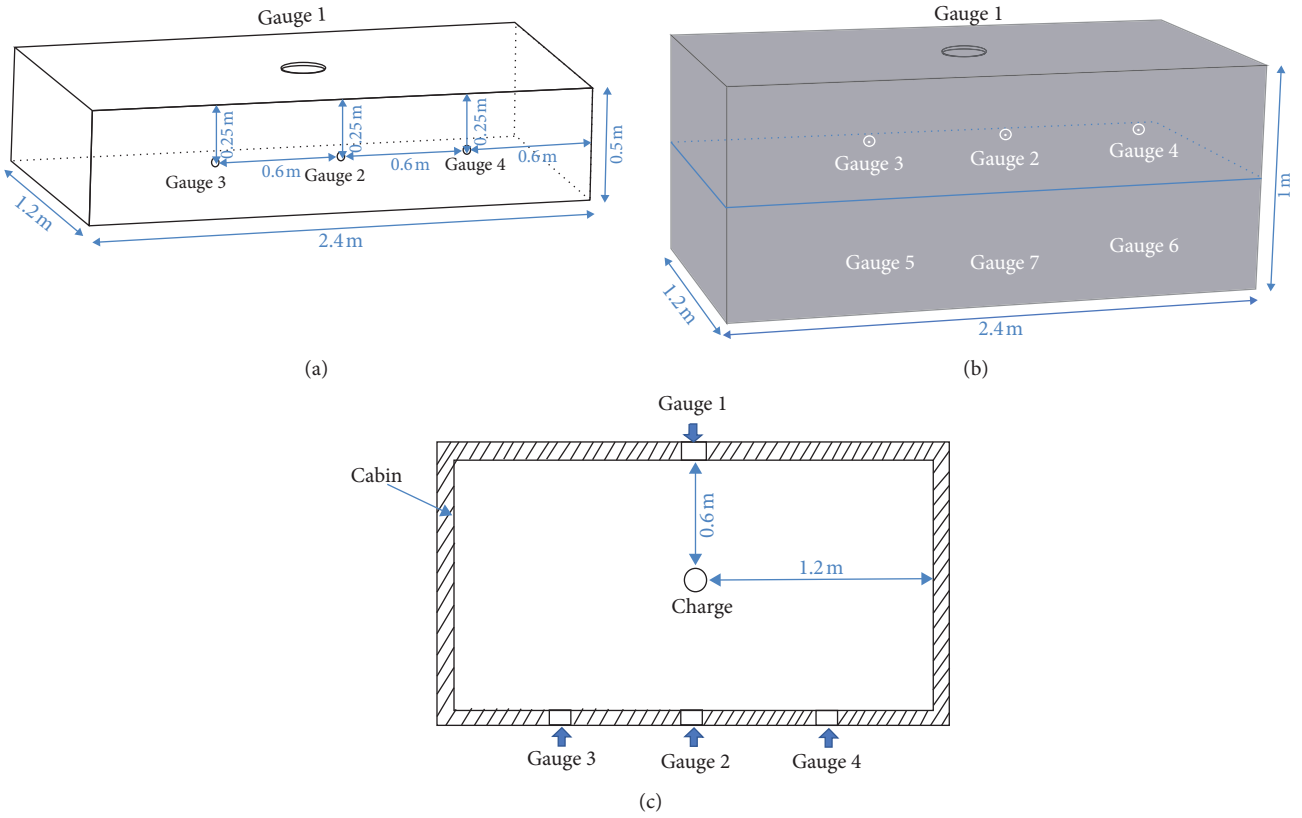

Figure 1: Schematic diagram of the simulated chamber layout. (a) Simulated chamber 1. (b) Simulated chamber 2. (c) Top view of simulation chamber.

(a) (b)

Figure 2: Photograph of simulated chambers. (a) Simulated chamber 1. (b) Simulated chamber 2.

the chamber. The chamber was made of Q235 steel. As shown in Figure 2(b), the size of simulated chamber 2 was 2.4 m × 1.2 m × 1 m, and the chamber material was Q235 steel. The wall thickness of the main chamber in the upper level was 16 mm, the same as the design parameter of simulated chamber 1. The interior spatial volume of the lower adjacent chamber was the same as that of the upper main chamber, the bulkhead thickness was 6 mm, and the diameter of the circular hole at the top of the main chamber was 120 mm. The explosive charge was placed at the geometric center of the main chamber through the top round hole. A 200 mm diameter prefabricated round hole was opened between the two chambers to ensure that explosive products in the main chamber could move into the adjacent chamber during the explosion process. The test charges were 418 g of TNT bare charges fabricated into cylindrical charges of equal height (ϕ70 mm × 68 mm).

At the test point for shock wave load measurement, a Model CY-YD-203T sensor produced by Lianneng Electronic Technology Co., Ltd. (Yangzhou, Jiangsu Province, China) was used. Its parameters were as follows: range 0–30 MPa, output voltage 0–5 V, operating temperature −40–150°C, and response frequency 100 kHz. At the test point for quasistatic pressure measurement, a Model CY-YZ-010 sensor produced by Lianneng Electronic Technology Co., Ltd., was used. The parameters were ranging 0–1 MPa,

output voltage 0–5 V, operating temperature −40°–85°C, and response frequency 2 kHz. The measurement system consisted mainly of a data acquisition system and a charge amplifier. The data acquisition equipment was a Model IDH446 data acquisition instrument produced by LDS Company of the United Kingdom, and the charge amplifier was a Model YE5853 charge amplifier produced by Lianneng Electronic Technology Co., Ltd., in Yangzhou, Jiangsu. At the shock wave test point, the sensor was connected to the charge amplifier, its sensitivity setting was consistent with that of the sensor, and the amplification factor was set to 1. The charge amplifier was connected to the data acquisition instrument, with the sampling frequency of the two shock wave signal channels set at 10 MHz. The sensor at the quasistatic pressure test point was connected directly to the data acquisition instrument, the sampling frequency of the two quasistatic pressure signal channels was set to 10 kHz, and the data recording was triggered by the rising edge of the channel.

The test site was prepared before the initiation of the experiment, including the placement of the test system and the installation of the circuits and sensors. At the placement location of the simulated chamber, the ground was leveled with a bulldozer and then covered with fine sand to damp the mechanical vibrations of the simulated chamber in the explosion. The simulated chamber was placed on the sand with a crane, and the layout position was kept level. After the placement of the chamber, the sensors were installed. At the shock wave test point, the sensor was placed in the through-hole reserved on the chamber bulkhead. An elastic and insulating nylon fixture was installed between the sensor and the bulkhead to effectively block the stress waves and interference signals, such as mechanical vibrations and electrical signals. The sensor was housed in the nylon fixture, and the nylon sleeve was installed in the through-hole of the bulkhead with an interference fit to ensure a tight fit. The pressure sensitive surface of the sensor was flush with the inner surface of the bulkhead, and the wiring was fastened to prevent movement. A metal buckle cap was installed at the end of the nylon sleeve to hold the entire fixture in place. At test points for quasistatic pressure measurement, nylon sleeve tooling was also installed, but the tooling was screwed into the hole on the bulkhead to ensure effective isolation against mechanical vibrations, electrical signals, and stress waves. Finally, the charge amplifier and the digital data acquisition were grounded. The power line and the test data line were separated, and the data lines were kept knot-free wherever possible.

3.2. Analysis of Experimental Results. Following the above-mentioned experimental method, we conducted four explosion tests in two simulated chambers and statistically analyzed the experimental data by deleting invalid data and averaging the effective data. We then analyzed the shock wave load data and the quasistatic pressure load data separately.

3.2.1. Shock Wave Load. For the shock wave load of the two simulated chambers, the mass of the explosive and the distance from the test point to the detonation point were the same. The shock wave pressure-time (p-t) curves obtained in the two simulated chambers in the experiment are shown in Figure 3.

As can be seen from Figure 3, the peak value of the shock wave overpressure was about 10 MPa, the positive pressure action time was about 0.1 ms, and the specific impulse was about 900 Pa·s. In identical simulation chambers, the two test points were operating in parallel, and the shock wave load parameters obtained at the two test points were consistent, indicating that the experimental data were valid and accurate. The results in Figure 3(c) show that, at the shock wave test point in the lower level of simulated chamber 2, only interference clutter signals were acquired, indicating that the shock wave load from the explosion in the upper level did not affect the lower chamber structure after the explosion. To compare simulated chamber 1 and simulated chamber 2, we list the shock wave load parameters in Table 1. The shock wave load parameters in the two chambers were not different, indicating that when the main chamber was partially damaged, the adjacent chamber did not affect the shock wave load in the main chamber. This is because the main effect of the adjacent chamber on the main chamber was the outflow of explosion products. Since the shock wave propagation velocity was very high, the explosion products did not have time to flow to the adjacent chamber when the shock wave exerted its load on the chamber wall. As a result, the shock wave loads of the two simulated chambers were very similar.

The two shock wave test points in the experiment were both positions of positive reflection of the shock wave. The calculation method for the first positively reflected shock wave pressure is well-established and is usually based on the pressure of the incident shock wave. In this paper, we chose to use the Brode formula with a larger range of application to calculate the positive reflected shock wave overpressure [4]:

$$\frac{p_r}{p_s} = \frac{2.655 \times 10^{-3} p_s}{1 + 1.728 \times 10^{-4} p_s + 1.921 \times 10^{-9} p_s} + 2 + \frac{4.218 \times 10^{-3} + 4.834 \times 10^{-2} p_s + 6.856 \times 10^{-6} p_s^2}{1 + 7.997 \times 10^{-3} p_s + 3.833 \times 10^{-6} p_s^2}, \quad (1)$$

where p_r is the peak overpressure (MPa) of the reflected shock wave and p_s is the peak overpressure (MPa) of the incident wave.

In order to calculate the pressure of the reflected shock wave, one must first calculate the incident shock wave pressure. The incident pressure was obtained from the Henrych formula:

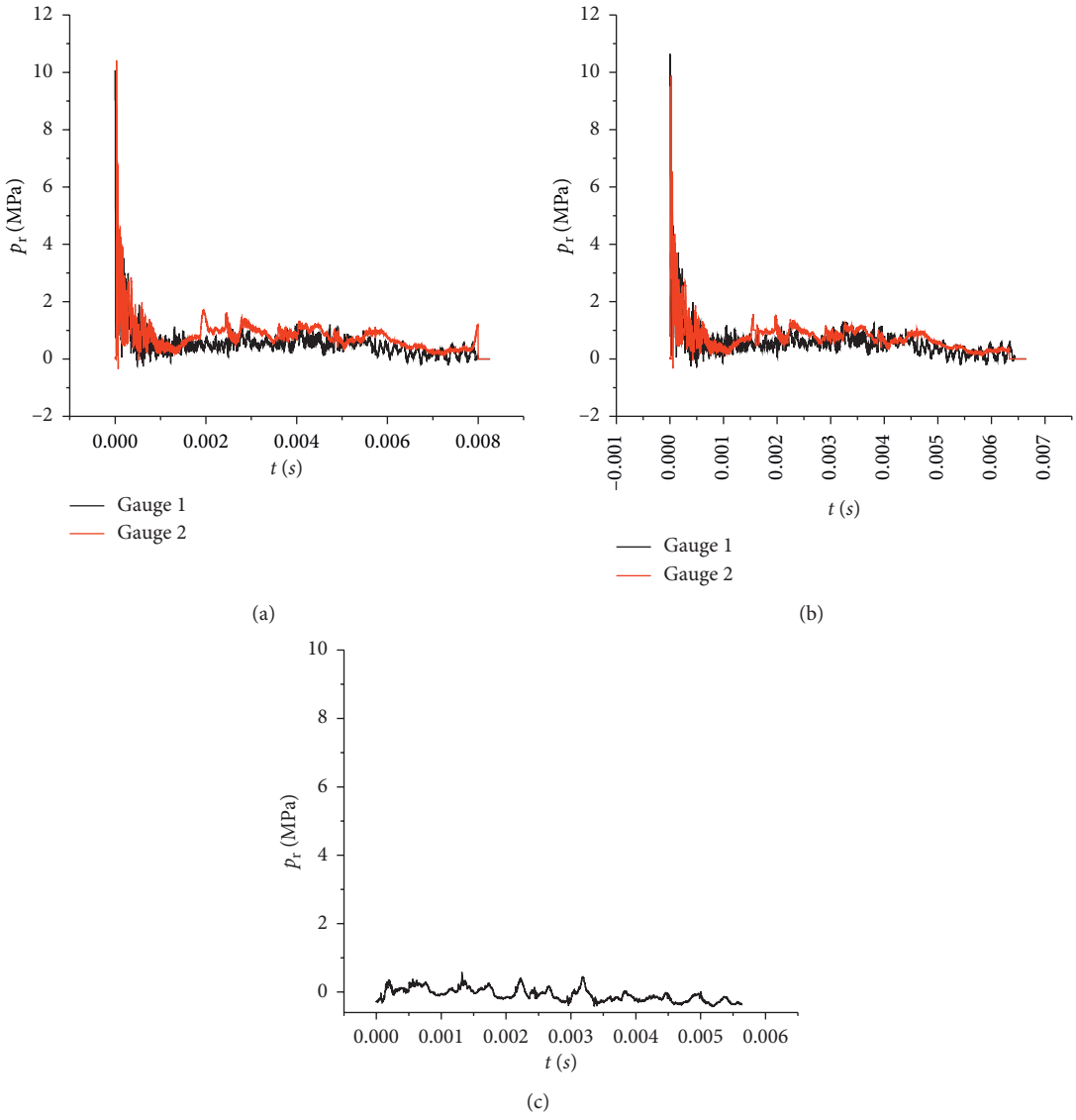

Figure 3: Shock wave load p-t curve. (a) Simulated chamber 1. (b) Simulated chamber 2, upper level. (c) Simulated chamber 2, lower level.

Table 1: Shock wave load parameters.

Simulated chamber	Test point	Peak value of overpressure (MPa)	Positive pressure reaction time (s)	Specific impulse (Pa·s)
1	1	10.06	0.00098	897.5
	2	10.40	0.00097	899.8
2	1	10.64	0.00096	902.3
	2	9.87	0.00112	913.8
	7	0	0	0

$$p_s = \frac{1.407\,17}{\overline{R}} + \frac{0.553\,97}{\overline{R}^2} - \frac{0.035\,72}{\overline{R}^3} + \frac{0.000\,625}{\overline{R}^4}, \quad 0.05 \le \overline{R} \le 0.3,$$

$$p_s = \frac{0.619\,38}{\overline{R}} - \frac{0.032\,62}{\overline{R}^2} + \frac{0.213\,24}{\overline{R}^3}, \quad 0.3 \le \overline{R} \le 1, \tag{2}$$

$$p_s = \frac{0.066\,2}{\overline{R}} + \frac{0.405}{\overline{R}^2} + \frac{0.328\,8}{\overline{R}^3}, \quad 1 \le \overline{R} \le 10,$$

$$\overline{R} = \frac{R}{\sqrt[3]{W}}, \tag{3}$$

where $\overline{R}$ is the proportional distance, R is the distance from the center of the explosion (m), and W is the TNT equivalent (kg).

We calculated the theoretical value of the peak overpressure for the conditions of this experiment. From equation (2), the peak overpressure of the incident wave was calculated to be 1.134 MPa. The peak overpressure of the reflected wave was then calculated from equation (1), and both the calculated and experimental results are listed in Table 2.

The compiled results in Table 2 show that the discrepancy between the theoretical calculation and experimental value of the shock wave load in the main chamber of simulated chamber 1 and simulated chamber 2 did not exceed 10%, which further proves that the presence of the adjacent chamber did not affect the shock wave in the main chamber. The shock wave load of an internal explosion in a chamber containing an adjacent chamber can be calculated using the explosive mass and the explosion distance as inputs.

3.2.2. Quasistatic Pressure Load. Having completed the analysis of shock wave load, the quasistatic pressure load is analyzed below. Figure 4 shows a typical quasistatic pressure p-t curve obtained in simulated chamber 1 in the experiment.

As shown in Figure 4, the quasistatic pressure sensor functioned normally and obtained valid test data. The quasistatic pressure load parameters were read from the p-t curve: the peak value of the overpressure was 0.89 MPa, the peak time was 0.029 s, the positive pressure reaction time was 0.67 s, and the specific impulse was 195,250.1 Pa·s. Compared with the shock wave signal, the peak value of the quasistatic pressure was very small, but the positive pressure reaction time and the specific impulse were much greater. In this experiment, the experimental data of the pressure load inside simulated chamber 1 mainly described the experimental load inside simulated chamber 2. We now analyze the quasistatic pressure load of the main chamber in simulated chamber 1 and simulated chamber 2. The experimental data are shown in Figure 5.

The quasistatic pressure p-t curves obtained in the two chambers are shown in Figure 5. The quasistatic pressure load parameters for the main chamber of simulated chamber 2 can be read from the p-t curves: the peak value of overpressure was 0.55 MPa, the peak time was 0.012 s, the positive pressure reaction time was 0.86 s, and the specific impulse was 143,443.1 Pa·s. Compared with the quasistatic pressure load parameters in simulated chamber 1, the peak value of the quasistatic overpressure of the main chamber of simulated chamber 2 was lower than that in simulated chamber 1. In terms of the total volume of the simulated chambers, the total volume of simulated chamber 2 was equivalent to twice of that of simulated chamber 1, so, for the same amount of explosive, the quasistatic overpressure peak in the main chamber of simulated chamber 2 was lower. The quasistatic pressure peak time of the main chamber of simulated chamber 2 was lower than that of simulated chamber 1. Other than the fact that simulated chamber 2 had a large total volume, the movement behavior of the internal product gas was also more complex, so its quasistatic pressure reached the peak value faster. The positive pressure reaction time of the quasistatic pressure of the main chamber of simulated chamber 2 was higher than that of simulated chamber 1. For the same area of the pressure relief hole, the positive pressure reaction time was inversely proportional to the volume of the space, so the pressure relief time was longer for simulated chamber 2. Specific impulse is a quantity derived from the overpressure peak and the positive pressure reaction time. Although the main chamber of simulated chamber 2 had a longer positive pressure reaction time, it had a lower peak value, so its specific impulse was lower than that of simulated chamber 1.

Having comparatively analyzed the quasistatic pressure load parameters in the main chambers of simulated chamber 1 and simulated chamber 2, we now analyze the quasistatic pressure load of the main chamber and the adjacent chamber of simulated chamber 2. The experimental data are displayed in Figure 6.

Figure 6 shows the quasistatic pressure load parameters of the adjacent chamber of simulated chamber 2: the overpressure peak was 0.40 MPa, the overpressure peak time was 0.045 s, the positive pressure reaction time was 0.86 s, and the specific impulse was 134,600.0 Pa·s. The peak value of quasistatic overpressure of the main chamber was higher than that of the adjacent chamber, and the peak time was shorter than that of the adjacent chamber. This is mainly because, with the explosive charge detonated in the main chamber, it takes time for the explosion product gas to move from the upper level to the lower level. When the quasistatic pressure reaches the peak in the adjacent chamber, some of

Table 2: Comparison of experimental value and theoretical value of peak shock wave overpressure in two simulated chambers.

Simulated chamber	Experimental value (MPa)	Calculated value (MPa)	Relative error
1	10.36	9.92	−4.25%
2	10.04	9.92	−1.19%

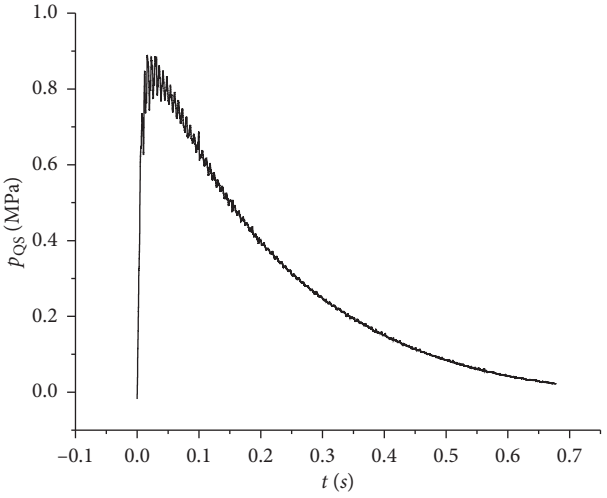

Figure 4: Quasistatic pressure p-t curve of simulated chamber 1.

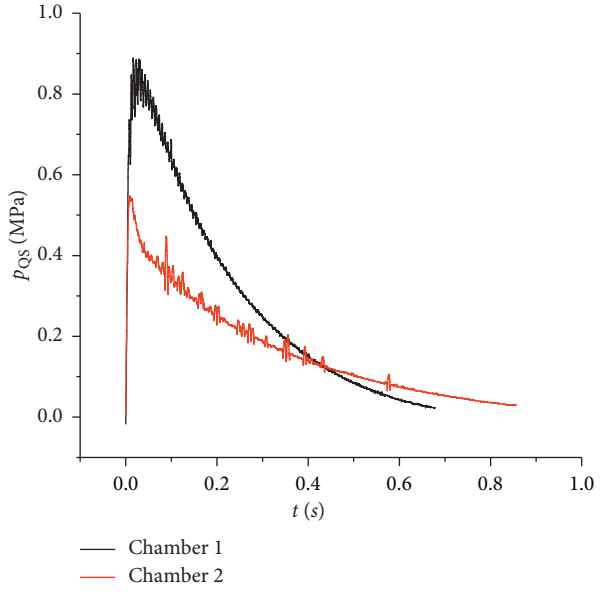

Figure 5: Quasistatic pressure p-t curves of simulated chamber 1 and simulated chamber 2.

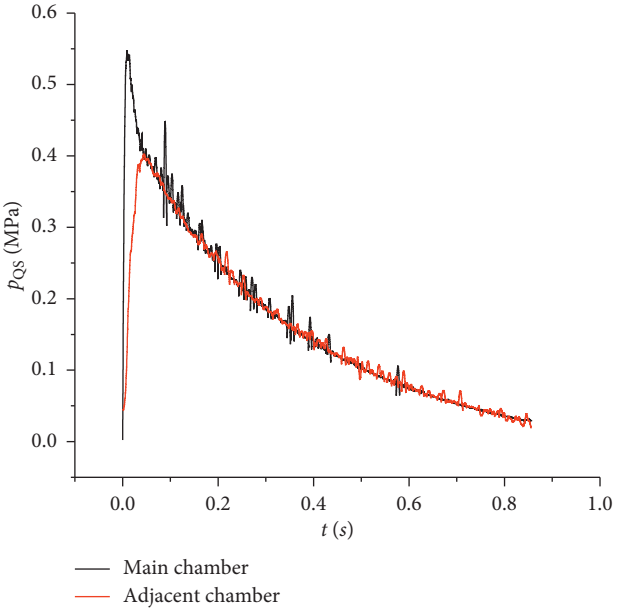

Figure 6: Quasistatic pressure p-t curves of the main chamber and adjacent chamber in simulated chamber 2.

the product gas has already been discharged from the pressure relief hole at the top of the chamber, so the peak value of the overpressure in the adjacent chamber is lower and lags behind in time. The quasistatic pressure in the main chamber quickly dissipates before the quasistatic pressure in the adjacent chamber peaks. This is because, while the gas movement in the main chamber stabilizes, the gas in the main chamber is escaping through the pressure relief holes at the top and the bottom simultaneously. After the explosion gas has stabilized in the chambers on the two levels, the explosion product gas has escaped through the pressure relief hole at the top of the chamber, so the pressure relief trend of the two chambers is basically the same, that is, the positive pressure reaction time is the same. Due to the difference of the overpressure peak, the specific impulse in the main chamber is greater than that in the adjacent chamber.

Having analyzed the quasistatic pressure load characteristics in the simulated chamber with an adjacent chamber, we now invoke the classical formula to calculate the quasistatic pressure load parameters of the experiment and compare the results with the experimental data. The peak value of the quasistatic overpressure depends on two parameters: the total energy released by the explosion and the volume of the chamber. In this paper, we used the formula in the UFC (Unified Facilities Criteria) manual [11] to calculate the peak value of the quasistatic overpressure:

$$p_{QS} = 2.26\left(\frac{m}{V}\right)^{0.7}. \quad (4)$$

This formula includes the chamber volume V (m^3), the explosive mass m (kg), and the peak overpressure of the quasistatic pressure P_{QS} (MPa).

Based on the operating conditions of this experiment, the corresponding theoretical values of quasistatic overpressure peaks were calculated. The theoretically calculated results and experimental results are listed in Table 3.

Table 3: Comparison of experimental and calculated values of quasistatic peak pressure.

Simulated chamber	Experimental value (MPa)	Calculated value (MPa)	Relative error (%)
1	0.88	0.95	+7.95
Main chamber of 2	0.55	0.58	+5.45
Adjacent chamber of 2	0.45	0.58	+28.9

It can be seen from Table 3 that the relative error between the calculated value and the experimental value of the peak value of quasistatic overpressure in the main chambers of simulated chamber 1 and simulated chamber 2 was less than 10%, and the calculation accuracy was good. The relative error of the calculated and experimental values for the adjacent chamber of simulated chamber 2 was 28.9%. This relatively large calculation error indicates that, during the flow process of explosion product from the main chamber to the adjacent chamber of simulated chamber 2, a portion of the gas products escaped through the top vent hole of the chamber, which made the calculated peak value of quasistatic overpressure in the adjacent chamber too high. In addition, compared to the adjacent chamber, the calculation error was smaller for the main chamber. This indicates that the presence of an adjacent chamber does not affect the theoretical peak value of quasistatic overpressure in the main chamber. That is, the peak value of quasistatic overpressure in the adjacent chamber can be calculated using the explosive mass and the chamber volume as inputs.

4. Conclusion

In this study, we analyzed the characteristics of the two types of loads formed by internal explosion in the adjacent chamber: the first reflected shock wave and the quasistatic pressure. We carried out explosion experiments in simulated chambers and obtained valid experimental data. We analyzed and compared the experimental values of the pressure load and the computed values obtained using the classical model. The results supported the following conclusions:

(1) When the main chamber is partially damaged by the explosion load, the adjacent chamber is basically unaffected by the shock wave loading, and the experienced quasistatic pressure load is less than that in the main chamber.

(2) The presence of the adjacent chamber does not affect the shock wave load in the main chamber, and the explosion shock wave load in the main chamber can be calculated using the mass of the explosive and the explosion distance as inputs.

(3) Since the explosive product gas is discharged through the vent hole of the chamber, the theoretically calculated result of the peak quasistatic overpressure in the adjacent chamber is high. The presence of the adjacent chamber does not affect the theoretical calculation of the peak quasistatic overpressure in the main chamber; that is, the peak quasistatic overpressure of the main chamber can be calculated using the explosive mass and the volume of the chamber as inputs.

Data Availability

The datasets supporting the conclusions of this article are available from the corresponding author upon request.

Conflicts of Interest

The authors declare that they do not have any commercial or associative interest that represents conflicts of interest in connection to the work submitted.

Acknowledgments

This work was supported by National Program on Key Basic Research Project of China (613305).

References

[1] M. Dorn, M. Nash, G. Anderson, N. Jones, and C. A. Brebbia, "The numerical prediction of the collapse of a complex brick building due to an internal explosion," *Pressure Vessels & Piping Division*, American Society of Mechanical Engineers (ASME), vol. 351, , pp. 349–358, 1996.

[2] B. M. Luccioni, R. D. Ambrosini, and R. F. Danesi, "Failure of a reinforced concrete building under blast loads," *WIT Transactions in Engineering Sciences*, vol. 49, pp. 336–345, 2006.

[3] W. S. Filler, "Post-detonation pressure and thermal studies of solid high explosives in a closed chamber," *Symposium (International) on Combustion*, vol. 6, no. 1, pp. 648–657, 1957.

[4] W. E. Baker, P. A. Cox, P. S. Westine, J. J. Kulesz, and R. A. Strehlow, *Explosion Hazards and Evaluation*, Elsevier, Amsterdam, 1983.

[5] G. F. Kinney, *Explosive Shocks in Air*, Macmillan, New York, NY, USA, 1962.

[6] M. Y. H. Bangash, *Impact and Explosion. Analysis and Design*, Spon Press: Blackwell Scientific Publications, Oxford, UK, 1993.

[7] M. Michael and A. Swisdak Jr., "Explosion effects in air," *Technical Report Naval Surface Weapons Center*, White Oak Laboratory, Washington, DC, USA, 1975.

[8] R. E. Shear and R. C. Makino, "A non-linear shock wave reflection theory," Pentagon Report Number: 0549946, Ballestic Research Laboratiers, Maryland, CO, USA, 1967.

[9] W. A. Keenan and J. E. Tancreto, *Blast Environmental for Fully and Partially Vented Explosion in cubicles*, Civil Engineering Laboratory, Dover, NJ, US, 1975.

[10] C. N. Kingery, R. N. Schumacher, and W. Ewing, "Internal pressure from explosions in suppressive structures," Ballistic Research Laboratory, Aberdeen, WA, USA, ADA019026, 1978.

[11] UFC 3-340-02 (Unified Facilities Criteria), *Structures to Resist the Effects of Accidental Explosions*, Dept. of the Army, the NAVY and the Air Force, Washington, DC, USA, 2008.

[12] TM-5-855-1, *Fundamentals of Protective Design for Conventional Weapons*, Department of Army, Washington, DC, USA, 1986.

[13] AASTP-1, *Manual of NATO Safety Principles for the Storage of Military Ammunition and Explosives*, NATO International Staff – Defense Investment Division, Brussels, Belgium, 2006.

[14] W. E. Baker, "Prediction and scaling of reflected impulse from strong blast waves," *International Journal of Mechanical Sciences*, vol. 9, no. 1, pp. 45–51, 1967.

[15] J. M. K. Chock and R. K. Kapania, "Review of two methods for calculating explosive air blast," *The Shock and Vibration Digest*, vol. 33, no. 2, pp. 91–102, 2001.

[16] F. Rigas and S. Sklavounos, "Experimentally validated 3-D simulation of shock waves generated by dense explosives in confined complex geometries," *Journal of Hazardous Materials*, vol. 121, no. 1-3, pp. 23–30, 2005.

[17] C. D. Eamon, "Reliability of concrete masonry unit walls subjected to explosive loads," *Journal of Structural Engineering*, vol. 133, no. 7, pp. 935–944, 2007.

[18] J. L. O'Daniel and T. Krauthammer, "Assessment of numerical simulation capabilities for medium–structure interaction systems under explosive loads," *Computers and Structures*, vol. 63, no. 5, pp. 875–887, 1997.

[19] S. Sklavounos and F. Rigas, "Computer-aided modeling of the protective effect of explosion relief vents in tunnel structures," *Journal of Loss Prevention in the Process Industries*, vol. 19, no. 6, pp. 621–629, 2006.

[20] J. Dragos, C. Wu, and D. J. Oehlers, "Simplification of fully confined blasts for structural response analysis," *Engineering Structures*, vol. 56, no. Complete, pp. 312–326, 2013.

[21] H. R. W. Weibull, "Pressures recorded in partially closed chambers at explosion of tnt charges," *Annals of the New York Academy of Sciences*, vol. 152, no. 1, pp. 357–361, 1968.

[22] J. F. Proctor and W. S. Filler, "A computerized technique for blast loads from confined explosions," in *Proceedings of Minutes of the Fourteenth Annual Explosions Safety Seminar*, pp. 99–124, New Orleans, LA, US, November 1972.

[23] C. E. Anderson, W. E. Baker, D. K. Wauters, and B. L. Morris, "Quasi-static pressure, duration, and impulse for explosions (e.g. HE) in structures," *International Journal of Mechanical Sciences*, vol. 25, no. 6, pp. 455–464, 1983.

[24] I. Edri, Z. Savir, V. R. Feldgun, Y. S. Karinski, and D. Z. Yankelevsky, "On blast pressure analysis due to a partially confined explosion: I. Experimental studies," *International Journal of Protective Structures*, vol. 2, no. 1, pp. 1–20, 2011.

[25] Z. Savir, I. Edri, V. R. Feldgun, Y. S. Karinski, and D. Z. Yankelevsky, "Blast pressure distribution on interior walls due to a partially confined explosion," in *Proceedings of international workshop on structure response to impact and blast (IWSRIB)*, Haifa, Israel, November 2009.

[26] I. Edri, V. R. Feldgun, Y. S. Karinski, and D. Z. Yankelevsky, "On blast pressure analysis due to a partially confined explosion: III. Afterburning effect," *International Journal of Protective Structures*, vol. 3, no. 3, pp. 311–331, 2012.

[27] V. R. Feldgun, Y. S. Karinski, I. Edri, and D. Z. Yankelevsky, "Prediction of the quasi-static pressure in confined and partially confined explosions and its application to blast response simulation of flexible structures," *International Journal of Impact Engineering*, vol. 90, no. 15, pp. 46–60, 2016.

[28] C. Wu, M. Lukaszewicz, K. Schebella, and L. Antanovskii, "Experimental and numerical investigation of confined explosion in a blast chamber," *Journal of Loss Prevention in the Process Industries*, vol. 26, no. 4, pp. 737–750, 2013.

[29] Y. Hu, C. Wu, M. Lukaszewicz, J. Dragos, J. Ren, and M. Haskett, "Characteristics of confined blast loading in unvented structures," *International Journal of Protective Structures*, vol. 2, no. 1, pp. 21–43, 2011.

[30] M. Larcher, F. Casadei, and G. Solomos, "Influence of venting areas on the air blast pressure inside tubular structures like railway carriages," *Journal of Hazardous Materials*, vol. 183, no. 1-3, pp. 839–846, 2010.

[31] X. U. Wei-Zheng and W. U. Wei-Guo, "Effects of size of venting holes on the characteristics of quasi-static overpressure in confined space," *Chinese Journal of High Pressure Physics*, vol. 31, no. 5, pp. 619–628, 2017.

[32] W. Xu, W. Wu, and Y. Lin, "Numerical method and simplified analytical model for predicting the blast load in a partially confined chamber," *Computers & Mathematics with Applications*, vol. 76, no. 2, pp. 284–314, 2018.

[33] W. A. Tzcin'ski, C. Stanislaw, and P. Jozef, "Studies of the effect of particles size on non-ideal explosives performance," *Propellants, Explosives, Pyrotechnics*, vol. 33, no. 3, pp. 227–235, 2008.

[34] P.-g. Jin, W. Guo, J.-l. Wang et al., "Energy releasing characteristics of aluminum powder in HMX-based explosives," *Chinese Journal of Energetic Matterials*, vol. 23, no. 10, pp. 989–993, 2015.

[35] C.-h. Wang, S.-s. Wang, and J.-x. Zhang, "Pressure load characteristics of nonideal explosives in a simulation cabin," *Shock and Vibration*, vol. 2019, Article ID 6862134, 8 pages, 2019.

[36] C. H. Wang, S. H. Wang, and J. X. Zhang, "Research on testing method of explosion pressure in cabin," *Acta Armamentarii*, vol. 40, no. 5, pp. 1004–1010, 2019.